Revisiting the Balazs thought experiment in the case of a left-handed material: electromagnetic-pulse-induced displacement of a dispersive, dissipative negative-index slab

Kenneth J. Chau[1] and Henri J. Lezec[2]

[1]*School of Engineering, The University of British Columbia, Kelowna, British Columbia, Canada*

[2]*Center for Nanoscale Science and Technology, National Institute of Standards and Technology, Gaithersburg, Maryland, USA*

Abstract

We propose a set of postulates to describe the mechanical interaction between a plane-wave electromagnetic pulse and a dispersive, dissipative slab having a refractive index of arbitrary sign. The postulates include the Abraham electromagnetic momentum density, a generalized Lorentz force law, and a model for absorption-driven mass transfer from the pulse to the medium. These opto-mechanical mechanisms are incorporated into a one-dimensional finite-difference time-domain algorithm that solves Maxwell's equations and calculates the instantaneous force densities exerted by the pulse onto the slab, the momentum-per-unit-area of the pulse and slab, and the trajectories of the slab and system center-of-mass. We show that the postulates are consistent with conservation of global energy, momentum, and center-of-mass velocity at all times, even for cases in which the refractive index of the slab is negative or zero. Consistency between the set of postulates and well-established conservation laws reinforces the Abraham momentum density as the one true electromagnetic momentum density and enables, for the first time, identification of the correct form of the electromagnetic mass density distribution and development of an explicit model for mass transfer due to absorption, for the most general case of a ponderable medium that is both dispersive and dissipative.

INTRODUCTION

It is well known that light carries momentum [1] and can transfer momentum to ponderable media via radiation pressure [2, 3]. Within the framework of classical electrodynamics, the momentum of light in a ponderable medium has an electromagnetic component associated with the electromagnetic fields and a mechanical component associated with the action of the electromagnetic fields on the constituent atoms of a medium. There is ongoing debate over the correct form of the electromagnetic momentum in a dielectric medium. In 1908, Minkowski [4] first proposed an electromagnetic momentum density $\vec{G} = \vec{D} \times \vec{B}$, where $\vec{D}$ is the electric displacement field and $\vec{B}$ is the magnetic flux density. When a light pulse with free-space momentum p_0 enters into a lossless, non-dispersive dielectric medium of positive refractive index n, the Minkowski formulation predicts an increase in the electromagnetic component of the pulse momentum from p_0 to np_0 [5]. In 1909, Abraham [6] proposed an alternative electromagnetic momentum density $\vec{G} = (\vec{E} \times \vec{H})/c^2$, where $\vec{E}$ is the electric field, $\vec{H}$ is the magnetic field, and c is the speed of light in vacuum. When a light pulse enters a lossless, non-dispersive, positive-index dielectric medium, the Abraham formulation predicts a decrease in the electromagnetic component of the pulse momentum from p_0 in vacuum to p_0/n in the dielectric [5]. Neither the Minkowski form nor the Abraham form has been universally accepted as the true electromagnetic momentum density (see Ref. [7] and the references therein). In addition, several other forms of the electromagnetic momentum density have since been proposed [8–14], each purporting to be the correct formulation.

Any plausible description for the electromagnetic momentum of light requires that, in a thermodynamically closed system, momentum be conserved. Classical electromagnetic theory, however, cannot be used to prove the validity of one formulation of the electromagnetic momentum density over another [7]. Any expression for the electromagnetic momentum density can be deemed valid so long as a corresponding force equation is chosen such that, when applied to describe the interaction of light with ponderable media, global momentum is conserved [7, 15].

BALAZS THOUGHT EXPERIMENT

Although no electromagnetic momentum density form can be proven based on conservation of momentum alone, the elegant Balazs thought experiment [16] provides a compelling case for the derivation of an electromagnetic momentum density in a dielectric based on the additional postulates of conservation of center-of-mass velocity [17] and invariance of pulse mass. The experiment consists of a reflection-less, transparent, non-dispersive, massive, and rigid dielectric slab having positive refractive index n, thickness L, and mass M [Fig. 1]. The slab is initially at rest and has antireflection coatings on its entrance and exit facets. A plane-wave light pulse of mass m initially propagating in vacuum at c can either move through the slab or alongside the slab. In the absence of external forces, total momentum of the system is mc and the center-of-mass of the slab-pulse system moves with uniform velocity $mc/(m+M)$. If the pulse enters the slab, the velocity of the pulse slows down to c/n, which must be accompanied by a movement of the slab in the direction of pulse propagation to maintain a constant center-of-mass velocity of the system. When the pulse leaves the slab and recovers its free-space momentum, the momentum of the slab returns to zero. Analysis of the slab center-of-mass displacement before and after the pulse has interacted with the slab, along with the requirement of conservation of system center-of-mass velocity and invariance of the pulse mass, implies that the slab acquires a momentum $(1-1/n)mc$ while the pulse is fully contained in the slab. For global momentum to be conserved, the electromagnetic momentum of the pulse in the slab must then be mc/n, the only plausible momentum allowed in the Balazs thought experiment. This momentum is consistent with the Abraham form of the electromagnetic momentum density when applied to an electromagnetic pulse completely immersed in a lossless, non-dispersive dielectric slab [6]. Although elegant, one of the limitations of the thought experiment is that it is based on the analysis of the pulse before and after interacting with the slab and does not provide information on whether global momentum is conserved even when the pulse is immersed in the slab. Moreover, the Balazs thought experiment is applicable only in the highly restrictive case where the slab is reflection-less and non-dissipative.

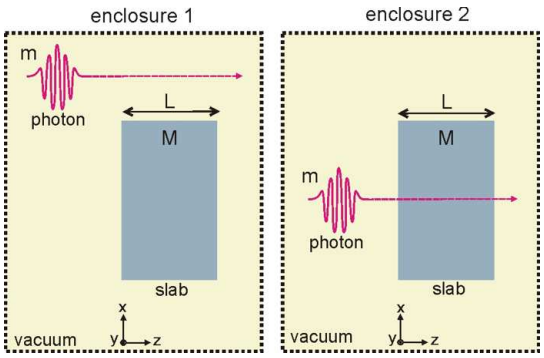

FIG. 1. Formulation of the Balazs thought experiment. Two identical enclosures each contain a photon of mass m and a non-dispersive, lossless slab of mass M and length L. (a) In enclosure 1, the photon propagates in a straight line above the slab through only vacuum. (b) In enclosure 2, the photon propagates in a straight line through both vacuum and the slab.

REVISITING THE BALAZS THOUGHT EXPERIMENT: NON-DISPERSIVE, POSITIVE-INDEX MEDIA

In our previous work [5], we re-visited the Balazs thought experiment using four postulates: Maxwell's equations to describe the propagation of electromagnetic fields, a generalized form of the Lorentz force law to describe the action of electromagnetic fields on ponderable media, the Abraham form of the electromagnetic momentum density, and conservation of both slab and pulse mass. The postulates were applied to describe, at all times, an electromagnetic plane-wave pulse traveling through a massive, dissipative, and positive-index slab of arbitrary complex relative permittivity and permeability. For the limiting case of a lossless slab, we analytically showed that global momentum and system center-of-mass velocity are conserved at all times, consistent with two of the starting postulates of the Balazs thought experiment. Invoking an additional mass transfer model to describe absorption, we numerically treated a number of test cases in which the slab possessed varying degrees of absorption (both with and without impedance matching to free space), verifying for all cases that conservation of momentum and center-of-mass velocity still held at all times.

OPTO-MECHANICAL INTERACTIONS IN DISPERSIVE, DISSIPATIVE, NEGATIVE-INDEX MEDIA

Materials in which both the real parts of the complex permittivity, $\underline{\epsilon}_r$, and complex permeability, $\underline{\mu}_r$, are positive, such as glass, are known as right-handed materials. A plane wave propagating in such a material has its electric field vector, magnetic field vector, and wavevector forming a right-handed triad. This leads to a wavevector and Poynting vector that are parallel and, as a result, co-linear phase and group velocities. In 1968, Veselago [18] studied a theoretical medium in which both the real parts of $\underline{\epsilon}_r$ and $\underline{\mu}_r$ are negative. A plane wave propagating in such a material has its electric field vector, magnetic field vector, and wavevector forming a left-handed triad (hence called a left-handed medium). This leads to a wavevector and Poynting vector that are anti-parallel and, as a result, contra-directional phase and group velocities. Although left-handed materials are not known to be naturally occurring, they have recently been implemented under the form of artificial metamaterials [19–22]. The optical properties of these artificial metamaterials (such as cloaking, lensing, and negative refraction) have received considerable attention, and only recently has their opto-mechanical properties become an area of interest [13, 18, 23, 24].

In this work, we examine the mechanical interaction between an electromagnetic pulse and a left-handed slab having real parts of $\underline{\epsilon}_r$ and $\underline{\mu}_r$ that are both negative. We also examine the limiting case in which the real parts of $\underline{\epsilon}_r$ and $\underline{\mu}_r$ are both zero, corresponding to a real part of the refractive index that is zero. To treat the case of a left-handed slab, we model a slab material possessing dispersion [25]. The dynamic interaction of an electromagnetic pulse with a dispersive slab is modeled using a set of postulates that includes Maxwell's equations, the Abraham electromagnetic momentum density, a generalized Lorentz force law, and a model for absorption in which mass is transferred from the pulse to the medium. Application of the postulates yields calculated quantities where global momentum and center-of-mass velocity are conserved at all times, regardless of the presence of loss and dispersion in the slab or the value and sign of the real part of the refractive index. Based on consistency with conservation of momentum and center-of-mass velocity, we infer that the Abraham electromagnetic momentum density and a generalized Lorentz force equation describe the electromagnetic and mechanical components, respectively, of light momentum in ponderable media, in agreement with theoretical arguments describing the interaction of electromagnetic waves with

materials having arbitrary polarization and magnetization densities [23, 24]. Demonstration that the Abraham momentum density, along with the aforementioned postulates, is the only plausible electromagnetic momentum density strengthens its case as the one true electromagnetic momentum density. Other significant outcomes of this work include the identification of an expression for the electromagnetic mass density distribution for the most general case of a dispersive, lossy material of arbitrary handedness and the development of a model for dynamic transfer of electromagnetic mass to absorbing media. It is also noteworthy that dispersion, treated here to accommodate materials with negative refractive index, was not explicitly treated in the original Balazs thought experiment. The thought experiment involved the comparison of the respective final positions of two otherwise indistinguishable pulses: one having traveled through only vacuum and the other having traveled through both vacuum and the slab. The assumption of indistinguishability between the two pulses implicitly precludes the possibility of dispersion.

FORMULATION OF POSTULATES

We first postulate that the propagation of electromagnetic fields is governed by Maxwell's equations relating the behavior of $\vec{E}$, $\vec{H}$, $\vec{D}$, and $\vec{B}$ to their sources, which include, in ponderable media, densities of polarization, $\vec{P}$, and magnetization, $\vec{M}$. In the absence of free charge density and free current density, the electromagnetic fields are related in real, time-domain notation by the Ampere-Maxwell law

$$\nabla \times \vec{H} = \frac{\partial \vec{D}}{\partial t} \tag{1}$$

and by Faraday's law

$$\nabla \times \vec{E} = -\frac{\partial \vec{B}}{\partial t}. \tag{2}$$

The electric displacement field is related to the polarization density via the relation

$$\begin{aligned} \vec{D} &= \epsilon_0 \vec{E} + \vec{P} \\ &= \epsilon_0 \vec{E} + \vec{P}_s + \vec{P}_d \\ &= \epsilon_0 \vec{E} + (\epsilon_\infty - 1)\, \epsilon_0 \vec{E} + \vec{P}_d, \end{aligned} \tag{3}$$

where ϵ_0 is the free-space permittivity, $\vec{P}_s = (\epsilon_\infty - 1)\epsilon_0 \vec{E}$ is the non-dispersive, frequency-independent component of the polarization density, $\vec{P}_d$ is the dispersive, frequency-dependent

component of the polarization density, and ϵ_∞ is the positive, static relative permittivity. Similarly, the magnetic flux density is related to the magnetization density via the relation

$$\begin{aligned}\vec{B} &= \mu_0\vec{H} + \vec{M} \\ &= \mu_0\vec{H} + \vec{M}_s + \vec{M}_d \\ &= \mu_0\vec{H} + (\mu_\infty - 1)\,\mu_0\vec{H} + \vec{M}_d,\end{aligned} \tag{4}$$

where μ_0 is the free-space permeability, $\vec{M}_s = (\mu_\infty - 1)\mu_0\vec{H}$ is the non-dispersive, frequency-independent component of the magnetization density, $\vec{M}_d$ is the dispersive, frequency-dependent component of the magnetization density, and μ_∞ is the positive, static relative permeability.

Temporal variation in $\vec{P}$ and $\vec{M}$ yield an electric current density $\vec{J}_e$ and a magnetic current density $\vec{J}_m$ given respectively by

$$\begin{aligned}\vec{J}_e &= \frac{\partial\vec{P}}{\partial t} \\ &= \frac{\partial\vec{D}}{\partial t} - \epsilon_0\frac{\partial\vec{E}}{\partial t}\end{aligned} \tag{5}$$

and

$$\begin{aligned}\vec{J}_m &= \frac{\partial\vec{M}}{\partial t} \\ &= \frac{\partial\vec{B}}{\partial t} - \mu_0\frac{\partial\vec{H}}{\partial t}.\end{aligned} \tag{6}$$

Parsing the current densities into non-dispersive and dispersive components, $\vec{J}_e$ and $\vec{J}_m$ can be re-expressed as

$$\begin{aligned}\vec{J}_e &= \vec{J}_{es} + \vec{J}_{ed} \\ &= \frac{\partial\vec{P}_s}{\partial t} + \frac{\partial\vec{P}_d}{\partial t} \\ &= \epsilon_0\,(\epsilon_\infty - 1)\,\frac{\partial\vec{E}}{\partial t} + \frac{\partial\vec{P}_d}{\partial t}\end{aligned} \tag{7}$$

and

$$\begin{aligned}\vec{J}_m &= \vec{J}_{ms} + \vec{J}_{md} \\ &= \frac{\partial\vec{M}_s}{\partial t} + \frac{\partial\vec{M}_d}{\partial t} \\ &= \mu_0\,(\mu_\infty - 1)\,\frac{\partial\vec{H}}{\partial t} + \frac{\partial\vec{M}_d}{\partial t},\end{aligned} \tag{8}$$

respectively, where $\vec{J}_{es} = \partial \vec{P}_s / \partial t$ is the non-dispersive component of the electric current density, $\vec{J}_{ed}$ is the dispersive component of the electric current density, $\vec{J}_{ms} = \partial \vec{M}_s / \partial t$ is the non-dispersive component of the magnetic current density, and $\vec{J}_{md}$ is the dispersive component of the magnetic current density.

We model $\vec{J}_{ed}$ and $\vec{J}_{md}$ using general first-order differential equations given by [25, 26]

$$\frac{\partial \vec{J}_{ed}}{\partial t} + \Gamma_e \vec{J}_{ed} = \epsilon_0 \omega_{pe}^2 \vec{E} \tag{9}$$

and

$$\frac{\partial \vec{J}_{md}}{\partial t} + \Gamma_m \vec{J}_{md} = \mu_0 \omega_{pm}^2 \vec{H}, \tag{10}$$

respectively, where ω_{pe} is the electric resonance frequency, ω_{pm} is the magnetic resonance frequency, Γ_e is the electric damping factor, and Γ_m is the magnetic damping factor.

To investigate electromagnetic pulse interaction with a slab, we derive relations for the frequency-dependent complex permittivity and complex permeability of the slab medium in terms of the parameters in Eqs. (9) and (10). These relations will then be used to set $\underline{\epsilon}_r$ and $\underline{\mu}_r$ values over the frequency bandwidth of the pulse. Assuming time-harmonic dependence of the electric field $\vec{E} = \text{Re}[\underline{\vec{E}} e^{-i\omega t}]$ and magnetic field $\vec{H} = \text{Re}[\underline{\vec{H}} e^{-i\omega t}]$, where $\underline{\vec{E}}$ is the complex electric field, $\underline{\vec{H}}$ is the complex magnetic field, we re-cast the constitutive relations from real, time-domain notation [as given in Eqs. (9) and (10)] into complex, frequency-domain notation. The dispersive components of the complex electric current density, $\underline{\vec{J}}_{ed}$, and the complex magnetic current density, $\underline{\vec{J}}_{md}$, then become related to $\underline{\vec{E}}$ and $\underline{\vec{H}}$ by

$$\underline{\vec{J}}_{ed} = \frac{\epsilon_0 \omega_{pe}^2}{\Gamma_e - i\omega} \underline{\vec{E}} \tag{11}$$

and

$$\underline{\vec{J}}_{md} = \frac{\mu_0 \omega_{pm}^2}{\Gamma_m - i\omega} \underline{\vec{H}}, \tag{12}$$

respectively. Ampere-Maxwell's law in complex, frequency-domain notation is

$$\nabla \times \underline{\vec{H}} = -i\omega \underline{\vec{D}}. \tag{13}$$

where $\underline{\vec{D}}$ is the complex electric displacement field. Re-casting Eqs. (5) and (7) into complex, frequency-domain notation, we get expressions for the complex electric current density, $\underline{\vec{J}}_e$, given by

$$\underline{\vec{J}}_e = -i\omega \underline{\vec{D}} + i\omega \epsilon_0 \underline{\vec{E}} \tag{14}$$

and

$$\underline{\vec{J}}_e = -i\omega\epsilon_0 \left(\epsilon_\infty - 1\right) \underline{\vec{E}} + \underline{\vec{J}}_{ed}, \tag{15}$$

respectively.

Solving Eqs. (14) and (15) for $\underline{\vec{D}}$ and then substituting into Eq. (13) yields

$$\begin{aligned} \nabla \times \underline{\vec{H}} &= -i\omega\epsilon_\infty\epsilon_0\underline{\vec{E}} + \frac{\epsilon_0\omega_{pe}^2}{\Gamma_e - i\omega}\underline{\vec{E}} \\ &= -i\omega\epsilon_0 \left(\epsilon_\infty - \frac{\omega_{pe}^2}{\omega(\omega + i\Gamma_e)}\right) \underline{\vec{E}} \\ &= -i\omega\epsilon_0\underline{\epsilon}_r(\omega)\underline{\vec{E}}, \end{aligned} \tag{16}$$

where $\underline{\epsilon}_r(\omega)$ is the complex, frequency-dependent relative permittivity given by

$$\underline{\epsilon}_r(\omega) = \epsilon_\infty - \frac{\omega_{pe}^2}{\omega(\omega + i\Gamma_e)}. \tag{17}$$

Faraday's law in complex, frequency-domain notation is

$$\nabla \times \underline{\vec{E}} = i\omega\underline{\vec{B}}. \tag{18}$$

where $\underline{\vec{B}}$ is the complex magnetic flux density. Re-casting Eqs. (6) and (8) into complex, frequency-domain notation, we get expressions for the complex magnetic current density, $\underline{\vec{J}}_m$, given by

$$\underline{\vec{J}}_m = -i\omega\underline{\vec{B}} + i\omega\mu_0\underline{\vec{H}} \tag{19}$$

and

$$\underline{\vec{J}}_m = -i\omega\mu_0 \left(\mu_\infty - 1\right) \underline{\vec{H}} + \underline{\vec{J}}_{md}, \tag{20}$$

respectively.

Solving Eqs. (19) and (20) for $\underline{\vec{B}}$ and then substituting into Eq. (18) yields

$$\begin{aligned} \nabla \times \underline{\vec{E}} &= i\omega\mu_\infty\mu_0\underline{\vec{H}} - \frac{\mu_0\omega_{pm}^2}{\Gamma_m - i\omega}\underline{\vec{H}} \\ &= i\omega\mu_0 \left(\mu_\infty - \frac{\omega_{pm}^2}{\omega(\omega + i\Gamma_m)}\right) \underline{\vec{H}} \\ &= i\omega\mu_0\underline{\mu}_r(\omega)\underline{\vec{H}}, \end{aligned} \tag{21}$$

where $\underline{\mu}_r(\omega)$ is the complex, frequency-dependent relative permeability given by

$$\underline{\mu}_r(\omega) = \mu_\infty - \frac{\omega_{pm}^2}{\omega(\omega + i\Gamma_m)}. \tag{22}$$

The complex permittivity and complex permeability given in Eqs. (17) and (22) obey the Kramers-Kronig relation and satisfy causality [25].

To investigate both right-handed and left-handed materials, we adjust the parameters ϵ_∞, μ_∞, ω_{pe}, ω_{pm}, Γ_e, and Γ_m in Eqs. (17) and (22) so that $\underline{\epsilon}_r$ and $\underline{\mu}_r$ can have either positive or negative real parts. We restrict our treatment to consider cases in which the real parts of $\underline{\epsilon}_r$ and $\underline{\mu}_r$ are either both positive or both negative, reserving the cases of an electric conductor ($\mathrm{Re}[\underline{\epsilon}_r] < 0$ and $\mathrm{Re}[\underline{\mu}_r] > 0$) and a magnetic conductor ($\mathrm{Re}[\underline{\epsilon}_r] > 0$ and $\mathrm{Re}[\underline{\mu}_r] < 0$) for future study. Once the values of $\underline{\epsilon}_r$ and $\underline{\mu}_r$ are specified, the resulting complex refractive index is given by [27]

$$\underline{n}(\omega) = \mathrm{Sign}\left[\mathrm{Re}[\underline{\epsilon}_r(\omega)]|\underline{\mu}_r(\omega)| + \mathrm{Re}[\underline{\mu}_r(\omega)]|\underline{\epsilon}_r(\omega)|\right] \sqrt{\underline{\epsilon}_r(\omega)\underline{\mu}_r(\omega)}, \tag{23}$$

which typically has a positive real part when $\mathrm{Re}[\underline{\epsilon}_r] > 0$ and $\mathrm{Re}[\underline{\mu}_r] > 0$ and a negative real part when $\mathrm{Re}[\underline{\epsilon}_r] < 0$ and $\mathrm{Re}[\underline{\mu}_r] < 0$. We restrict our analysis to passive media that are either non-absorbing ($\mathrm{Im}[\underline{n}] = 0$) or absorbing ($\mathrm{Im}[\underline{n}] > 0$), not treating the case of active gain media ($\mathrm{Im}[\underline{n}] < 0$). Note that $\underline{\epsilon}_r(\omega)$ and $\underline{\mu}_r(\omega)$ include the effect of loss through Γ_e and Γ_m, are inherently dispersive, and can generally only achieve negative real values over a limited frequency range, all consistent with practical limitations of experimentally-implemented metamaterials.

Here, we postulate that the Abraham momentum density, shown earlier to be valid for non-dispersive materials [5], also applies to the case of a dispersive material having a real part of the refractive index that is either positive, negative, or zero. The electromagnetic momentum density is given at all points in space and time by

$$\vec{G} = \frac{\vec{E} \times \vec{H}}{c^2}. \tag{24}$$

We next consider the mechanical component of light momentum associated with the action of the electromagnetic fields on the atoms/molecules of a medium. We postulate that electromagnetic interaction with ponderable media is mediated via a generalized Lorentz force law first proposed by Einstein and Laub [28], and then recently studied by Mansuripur [29, 30]. The corresponding force density is given by

$$\vec{f} = (\vec{P} \cdot \nabla)\vec{E} + (\vec{M} \cdot \nabla)\vec{H} + \vec{J}_e \times \mu_0 \vec{H} - \vec{J}_m \times \epsilon_0 \vec{E}, \tag{25}$$

which provides a highly symmetric expression for the interaction of electric and magnetic fields with a material having non-zero polarization and magnetization densities. Here, as in

our previous work [5], we restrict the treatment to the case of an electromagnetic plane-wave normally incident onto a flat slab. When Eq. (25) is applied to this geometry, the first two terms vanish and it simplifies to

$$\vec{f} = \vec{J}_e \times \mu_0 \vec{H} - \vec{J}_m \times \epsilon_0 \vec{E}. \tag{26}$$

We note that Eq. (26) incorporates magnetization by the inclusion of an additional term involving $\vec{J}_m$, which differs from the conventional Lorentz force law which incorporates magnetization by the addition of $(\nabla \times \vec{M})/\mu_0$ to $\vec{J}_e$. As noted by Mansuripur [31], the use of the conventional Lorentz force law for media having non-zero magnetization density leads to the requirement of inelegant hidden momentum terms [32] to achieve conservation of global momentum.

We thus postulate that the electromagnetic component of the momentum density is described by Eq. (24) and the mechanical component is described by Eq. (25). Together, the electromagnetic momentum density and the force density can be expressed in the context of a momentum continuity equation [8, 33, 34]

$$\nabla \cdot \bar{\bar{T}} + \frac{\partial \vec{G}}{\partial t} = -\vec{f} \tag{27}$$

where $\bar{\bar{T}}$ is the stress tensor. The form of the corresponding stress tensor can be derived by inserting Eqs. (24) and (25) into Eq. (27), yielding

$$\nabla \cdot \bar{\bar{T}} = -(\vec{P} \cdot \nabla)\vec{E} - (\vec{M} \cdot \nabla)\vec{H} - \vec{J}_e \times \mu_0 \vec{H} + \vec{J}_m \times \epsilon_0 \vec{E} - \frac{\partial}{\partial t}\left(\frac{\vec{E} \times \vec{H}}{c^2}\right). \tag{28}$$

We use the relation $\epsilon_0 \mu_0 = 1/c^2$ and the definitions of the electric and magnetic current densities given by Eqs. (5) and (6), respectively, and develop the temporal derivative on the right hand side of Eq. (28) to give

$$\nabla \cdot \bar{\bar{T}} = -\nabla(\vec{P}\vec{E} + \vec{M}\vec{H}) - \frac{\partial \vec{P}}{\partial t} \times \mu_0 \vec{H} + \frac{\partial \vec{M}}{\partial t} \times \epsilon_0 \vec{E} - \epsilon_0 \frac{\partial \vec{E}}{\partial t} \times \mu_0 \vec{H} + \mu_0 \frac{\partial \vec{H}}{\partial t} \times \epsilon_0 \vec{E}. \tag{29}$$

Substituting Eqs. (3) and (4) into Eq. (29) yields

$$\nabla \cdot \bar{\bar{T}} = -\nabla(\vec{D}\vec{E} - \epsilon_0 \vec{E}\vec{E} + \vec{B}\vec{H} - \mu_0 \vec{H}\vec{H}) - \frac{\partial \vec{D}}{\partial t} \times \mu_0 \vec{H} + \frac{\partial \vec{B}}{\partial t} \times \epsilon_0 \vec{E}. \tag{30}$$

We invoke the Ampere-Maxwell law and Faraday's law and use the vector identity $\nabla(\vec{A} \cdot \vec{A})/2 = \vec{A} \times (\nabla \times \vec{A}) + (\vec{A} \cdot \nabla)\vec{A}$ to re-express Eq. (30) as

$$\nabla \cdot \bar{\bar{T}} = \nabla(-\vec{D}\vec{E} - \vec{B}\vec{H}) + \frac{1}{2}\nabla(\mu_0 \vec{H} \cdot \vec{H}) + \frac{1}{2}\nabla(\epsilon_0 \vec{E} \cdot \vec{E}). \tag{31}$$

The stress tensor can be directly identified from Eq. (31) as [33, 34]

$$\bar{\bar{T}} = -\vec{D}\vec{E} - \vec{B}\vec{H} + \frac{1}{2}(\mu_0 H^2 + \epsilon_0 E^2)\bar{\bar{I}}, \tag{32}$$

where $\bar{\bar{I}}$ is the identity matrix. The stress tensor given by Eq. (32) uniquely corresponds to the electromagnetic momentum density given by Eq. (24) and the force density given by Eq. (25). It should be noted that the momentum continuity equation does not a priori specify a particular combination of electromagnetic momentum density, force density, and stress tensor. Other combinations can be postulated which satisfy the momentum continuity equation, meaning that conservation of momentum alone is not a sufficiently stringent test to enable identification of a unique electromagnetic momentum density. However, imposing the simultaneous requirement of conservation of momentum and conservation of center of mass velocity may enable elimination of certain forms of the electromagnetic momentum density (and its corresponding force density and stress tensor), which would otherwise satisfy conservation of momentum. In Appendix A, we will examine the implications of selecting a Minkowski momentum density and its corresponding force density and stress tensor to study an electromagnetic plane-wave pulse normally incident onto a slab, showing that although global momentum is conserved, center of mass velocity is not conserved.

We next consider the flow of energy due to the propagation of the electromagnetic fields. We postulate that the rate of electromagnetic energy flow at all points in space and time is given by the Poynting vector

$$\vec{S} = \vec{E} \times \vec{H}. \tag{33}$$

The Poynting vector, in conjunction with Maxwell's equations, can be used to derive the electromagnetic mass density of the pulse [35], which is needed to calculate the center-of-mass of the pulse. Applying the divergence theorem to Eq. (33) and using Eqs. (1)–(4), we get

$$\begin{aligned}
\int_S (\vec{E} \times \vec{H}) \cdot d\vec{S} &= \int_V \nabla \cdot (\vec{E} \times \vec{H}) dV \\
&= \int_V [\vec{H} \cdot (\nabla \times \vec{E}) - \vec{E} \cdot (\nabla \times \vec{H})] dV \\
&= -\int_V (\mu_\infty \mu_0 \vec{H} \cdot \frac{\partial \vec{H}}{\partial t} + \vec{H} \cdot \vec{J}_{md} + \epsilon_\infty \epsilon_0 \vec{E} \cdot \frac{\partial \vec{E}}{\partial t} + \vec{E} \cdot \vec{J}_{ed}) dV.
\end{aligned} \tag{34}$$

Substituting the constitutive relations given by Eqs. (9) and (10) into Eq. (34) then yields

$$\int_S (\vec{E} \times \vec{H}) \cdot d\vec{S} = -\int_V [\mu_\infty \mu_0 \vec{H} \cdot \frac{\partial \vec{H}}{\partial t} + \frac{1}{\mu_0 \omega_{pm}^2} (\frac{\partial \vec{J}_{md}}{\partial t} + \Gamma_m \vec{J}_{md}) \cdot \vec{J}_{md} + \epsilon_\infty \epsilon_0 \vec{E} \cdot \frac{\partial \vec{E}}{\partial t} + \frac{1}{\epsilon_0 \omega_{pe}^2} (\frac{\partial \vec{J}_{ed}}{\partial t} + \Gamma_e \vec{J}_{ed}) \cdot \vec{J}_{ed}] dV. \tag{35}$$

Further developing Eq. (35) and separating the temporal derivative terms in the volume integral yields [36]

$$\begin{aligned} \int_S (\vec{E} \times \vec{H}) \cdot d\vec{S} + \int_V \left(\frac{\Gamma_e J_{ed}^2}{\epsilon_0 \omega_{pe}^2} + \frac{\Gamma_m J_{md}^2}{\mu_0 \omega_{pm}^2} \right) dV \\ = -\int_V \frac{\partial}{\partial t} \left(\frac{\mu_\infty \mu_0 H^2}{2} + \frac{\epsilon_\infty \epsilon_0 E^2}{2} + \frac{J_{ed}^2}{2\epsilon_0 \omega_{pe}^2} + \frac{J_{md}^2}{2\mu_0 \omega_{pm}^2} \right) dV \\ = -\int_V \frac{\partial W}{\partial t} dV, \end{aligned} \tag{36}$$

where the electromagnetic energy density of the electromagnetic fields at all points in space and time is given by

$$W = \frac{\mu_\infty \mu_0 H^2}{2} + \frac{\epsilon_\infty \epsilon_0 E^2}{2} + \frac{J_{ed}^2}{2\epsilon_0 \omega_{pe}^2} + \frac{J_{md}^2}{2\mu_0 \omega_{pm}^2}, \tag{37}$$

which is similar to the energy density formulation derived by Ruppin [35]. This expression simplifies to the well-known energy density expression for a plane wave in free space when $\epsilon_\infty = 1$, $\mu_\infty = 1$, $J_{ed} = 0$ and $J_{md} = 0$.

A valid description of electromagnetic pulse interaction with a ponderable slab should conserve the total mass of the system for all time. For the case of a pulse interacting with a lossless slab, conservation of total mass is satisfied by fixing the mass of the pulse and the mass of the slab. For the case of a pulse interacting with a lossy slab, conservation of total mass for all time requires dynamic and generally non-uniform exchange of mass from the pulse to the slab. Here, we postulate that the distribution of the pulse mass exchanged to the slab is based on the mass density distribution of the electromagnetic pulse. Generalizing the mass density, ρ, proposed for a pulse in a non-dispersive ponderable medium [5], we postulate that the mass density of the pulse in the present, more-general case of a dispersive material is given by

$$\rho = \frac{W}{c^2}. \tag{38}$$

We invoke local conservation of mass by implementing an incremental mass transfer model where, at any moment in time, the mass reduction of the pulse due to absorption in a

medium is compensated by an identical mass increase of the absorbing medium, distributed in space according to the instantaneous mass density distribution of the pulse given by Eqs. (37) and (38). The spatially distributed pulse mass transferred to the lossy slab affects the center-of-mass of the slab, which, in turn, determines the center-of-mass velocity of the system. It should be noted that invoking conservation of mass in this manner also ensures that the total energy of the system is conserved for all time.

METHODOLOGY

We verify the consistency of the complete set of aforementioned postulates with conservation laws for momentum and mass by subjecting them to a number of representative test cases where a pulse is incident onto a slab. Consistency of our postulates with conservation of momentum validates the chosen forms of the electromagnetic momentum density and opto-mechanical force density. Furthermore, consistency with conservation of center-of-mass velocity validates the chosen model for the spatio-temporal dependence of pulse mass density and mechanisms for pulse mass transfer to the slab in a dispersive and dissipative medium. The complete set of assumptions and postulates used in our analysis are summarized in Table I. The incident electromagnetic pulse consists of a sinusoidal carrier wave oscillating at a frequency $\omega_c = 6 \times 10^{14}\,\mathrm{Hz}$ (corresponding to a free-space wavelength $\lambda_0 = 500\,\mathrm{nm}$) and a Gaussian intensity envelope with a temporal full-width-at-half-maximum of 1.5 fs. A pulse is used, as opposed to a continuous wave, so that the center-of-mass of the electromagnetic fields are well-defined. The spectral contents of the pulse are centered about ω_c, as depicted in Fig. 2. The pulse propagates along the z-direction and is normally incident onto a flat slab occupying the region $0 < z < L = 750\,\mathrm{nm}$. The slab is composed of a dispersive dielectric characterized by a complex relative electric permittivity $\underline{\epsilon}_r$ and complex relative magnetic permeability $\underline{\mu}_r$, yielding a complex index of refraction given by Eq. (23). For initial simplicity of presentation, we eliminate the effect of reflection from the faces of the slab by assuming that the slab is impedance-matched to vacuum, which in our case can be achieved by setting $\underline{\epsilon}_r = \underline{\mu}_r$ to yield a relative impedance $\eta_r = \sqrt{\underline{\mu}_r/\underline{\epsilon}_r} = 1$. From Eq. (23), the assumption of impedance matching also sets $\underline{\epsilon}_r = \underline{\mu}_r = \underline{n}$. Impedance matching is not critical to our conclusions, and in Appendix B, we examine a case in which the slab material is non-impedance-matched ($\underline{\epsilon}_r \neq \underline{\mu}_r$) and show that similar results to

the impedance-matched cases are obtained. Here, we study five test cases in which the material parameters are varied such that the slab is either (1) positive index and lossless $[\underline{n}(\omega_c) = 1.47 + 0.00i]$, (2) positive index and lossy $[\underline{n}(\omega_c) = 1.42 + 0.34i]$, (3) negative index and lossless $[\underline{n}(\omega_c) = -1.53 + 0.00i]$, (4) negative index and lossy $[\underline{n}(\omega_c) = -1.53 + 0.34i]$, or (5) zero-index and lossless $[\underline{n}(\omega_c) = 0.00 + 0.00i]$. The values for the parameters ϵ_∞, μ_∞, ω_{pe}, ω_{pm}, Γ_e, and Γ_m corresponding to the five test cases are summarized in Table II. The resulting real and imaginary parts of $\underline{\epsilon}_r$, $\underline{\mu}_r$, and $\underline{n}$ for all test cases are depicted in Figs. 2(b), 2(c), and 2(d), respectively. Due to the dispersive nature of the constitutive relations, it is generally not possible to achieve a zero refractive index over the entire bandwidth of the pulse. We instead set the constitutive parameters so that the refractive index crosses zero at a frequency near the peak location of the pulse power spectrum.

The spatio-temporal evolution of the pulse is modeled using one-dimensional finite-difference time-domain (FDTD) solutions to Eqs. (1) and (2). The simulation space consists of a one-dimensional array of 17000 pixels, where pixels 1 to 2000 correspond to free-space, pixels 2001 to 17000 correspond to the slab, and pixels 17001 to 19000 correspond to free-space. The pixels in the free-space regions each have a size of 2 nm, and the pixels in the slab region each have a size of 0.05 nm. Perfectly-matched-layer boundary conditions are used at the two ends of the simulation space to eliminate spurious reflections from the boundaries. The temporal step size of the simulations is $0.05\,\text{nm}/(2c) = 8.3 \times 10^{-5}\,\text{fs}$, and the simulations are synchronized such that the time $t = 0$ coincides with the instant when the peak of the pulse is located at the front face of the slab. As shown in Fig. 3, we assume that $\vec{E}$ and $\vec{J}_e$ are oriented along the x-direction and $\vec{H}$ and $\vec{J}_m$ are oriented along the y-direction. The electric field is taken at the cell edge for integer time steps and the magnetic field is taken at the cell center for half-integer time steps. The electric and magnetic current densities are located together at the cell centers to achieve the matched medium conditions numerically. For a spatio-temporal grid with a spatial step size Δz, a spatial index i, a temporal step size Δt, and a temporal index n, we use the compressed notation $E_x(i\Delta z, (n+1)\Delta t) = E_x^{n+1}(i)$, $J_{e,x}((i+1/2)\Delta z, (n+3/2)\Delta t) = J_{e,x}^{n+3/2}(i+1/2)$, $H_y((i+1/2)\Delta z, (n+1/2)\Delta t) = H_y^{n+1/2}(i+1/2)$, and $J_{m,y}((i+1/2)\Delta z, (n+1)\Delta t) =$

TABLE I. Assumptions and postulates used in our analysis of electromagnetic pulse interaction with a slab. The quantities in the equations are defined in the text.

Explicit Force Density and Momentum Density Calculations

Assumptions	Postulates
• Slab is impedance-matched to vacuum • Slab is rigid and massive $M >> m$ • Pulse is a plane wave at normal incidence	• Two of Maxwell's equations: $\nabla \times \vec{H} = \partial\vec{D}/\partial t$ and $\nabla \times \vec{E} = -\partial\vec{B}/\partial t$ • Generalized Lorentz force law: $\vec{f} = \vec{J}_e \times \mu_0\vec{H} - \vec{J}_m \times \epsilon_0\vec{E}$ • Electromagnetic momentum density: $\vec{G} = \vec{E} \times \vec{H}/c^2$ • Poynting vector: $\vec{S} = \vec{E} \times \vec{H}$ • An incremental mass transfer model in which the pulse deposits mass in the slab with a distribution corresponding to the instantaneous mass density profile of the pulse

TABLE II. Parameters used in the FDTD simulations for the five test cases.

Test Case	$\epsilon_\infty, \mu_\infty$	ω_{pe}, ω_{pm} (rad/s)	Γ_e, Γ_m (rad/s)	$\underline{n}(\omega_c)$
1	4.00	6×10^{15}	0	$1.47 + 0.00i$
2	4.00	6×10^{15}	5×10^{14}	$1.42 + 0.34i$
3	1.00	6×10^{15}	0	$-1.53 + 0.00i$
4	1.00	6×10^{15}	5×10^{14}	$-1.57 + 0.34i$
5	2.53	6×10^{15}	0	$0.00 + 0.00i$

$J_{m,y}^{n+1}(i+1/2)$ [25]. The resulting discretized Maxwell's equations are then given by

$$
\begin{aligned}
H_y^{n+1/2}(i+1/2) &= H_y^{n-1/2}(i+1/2) - \frac{\Delta t}{\mu_0 \Delta z}\left[E_x^n(i+1) - E_x^n(i) + J_{m,y}^n(i+1/2)\Delta z\right] \\
J_{m,y}^{n+1}(i+1/2) &= \frac{1 - 0.5\Gamma_m \Delta t}{1 + 0.5\Gamma_m \Delta t} J_{m,y}^n(i+1/2) + \frac{\mu_0 \omega_{pm}^2 \Delta t}{1 + 0.5\Gamma_m \Delta t} H_y^{n+1/2}(i-1/2) \\
E_x^{n+1}(i) &= E_x^n(i) - \frac{\Delta t}{\epsilon_0 \Delta z}\left[H_y^{n+1/2}(i+1/2) - H_y^{n+1/2}(i-1/2)\right] \\
&\quad - \frac{1}{2}\frac{\Delta t}{\epsilon_0}\left[J_{e,x}^{n+1/2}(i+1/2) + J_{e,x}^{n+1/2}(i-1/2)\right] \\
J_{e,x}^{n+3/2}(i+1/2) &= \frac{1 - 0.5\Gamma_e \Delta t}{1 + 0.5\Gamma_e \Delta t} J_{e,x}^{n+1/2}(i+1/2) \\
&\quad + \frac{1}{2}\frac{\epsilon_0 \omega_{pe}^2 \Delta t}{1 + 0.5\Gamma_e \Delta t}\left[E_x^{n+1}(i) + E_x^{n+1}(i+1)\right]
\end{aligned}
\tag{39}
$$

RESULTS

We first examine the evolution of the electromagnetic fields of the pulse as it propagates through dispersive slabs with and without loss. Figures 4(a) and 4(c) display time-sequences of the FDTD-calculated electric fields for comparative cases in which a pulse is incident onto dispersive positive-index slabs with and without loss, respectively. The incident pulse consists of several electric field oscillations and has a width in vacuum comparable to the width of the slab, which enables the independent observation in time of the interaction of the leading and falling edges of the pulse with the front and back interfaces of the slab as well as that of the pulse with the interior of the slab while it is fully contained in the slab. Both impedance-matched slabs show no reflection from either of the two dielectric-vacuum interfaces. The pulse transmitted through the lossless slab is elongated and up-chirped

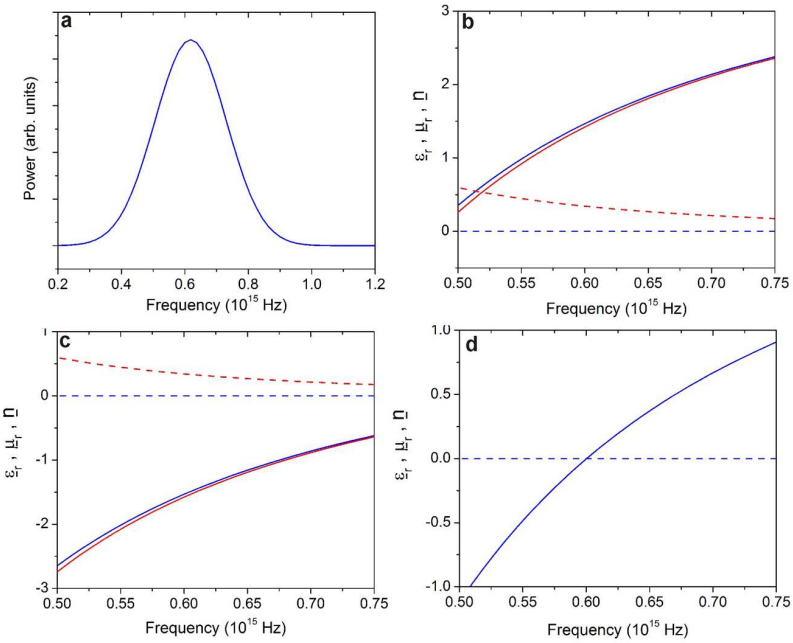

FIG. 2. (a) Power spectrum of the incident electromagnetic pulse. The complex refractive index of the slab is set by adjusting ϵ_∞, μ_∞, ω_{pe}, ω_{pm}, Γ_e, and Γ_m to vary the values of $\underline{\epsilon}_r$ and $\underline{\mu}_r$ over the bandwidth of the incident pulse. Under the assumption of impedance matching, $\underline{\epsilon}_r = \underline{\mu}_r = \underline{n}$. A positive-index is realized by setting $\mathrm{Re}[\underline{\epsilon}_r] > 0$ and $\mathrm{Re}[\underline{\mu}_r] > 0$ (right-handed material), a negative-index by setting $\mathrm{Re}[\underline{\epsilon}_r] < 0$ and $\mathrm{Re}[\underline{\mu}_r] < 0$ (left-handed material) and a zero-index by setting $\mathrm{Re}[\underline{\epsilon}_r] \simeq 0$ and $\mathrm{Re}[\underline{\mu}_r] \simeq 0$. The real (solid) and imaginary (dash) parts of $\underline{\epsilon}_r$, $\underline{\mu}_r$, and $\underline{n}$ for (b) test case 1 (blue) and test case 2 (red), (c) test case 3 and test case 4, and (d) test case 5. The material parameters corresponding to each of the test cases are summarized in Table II.

relative to the incident pulse due to dispersion in the slab, which causes spectral smearing of the pulse frequency components in the time domain. The pulse transmitted through the lossy slab, on the other hand, is significantly attenuated. Corresponding instantaneous force densities exerted by the pulse onto positive-index slabs without and with loss are depicted in Figs. 4(b) and 4(d), respectively. As shown in Figs. 5(a) and 5(c), similar trends in the electric field are observed when the pulse propagates through dispersive negative-index slabs with and without loss. Dynamic observation of the propagation of the pulse in the slab reveals backwards propagating phase fronts, as expected in a left-handed material. One difference in the instantaneous electric field distributions observed here from those

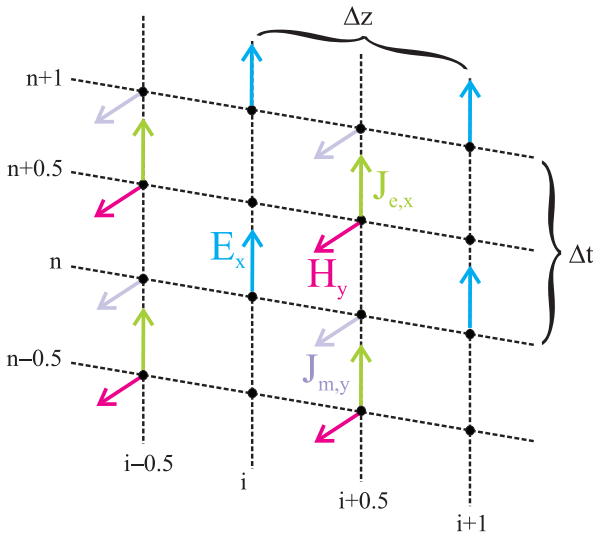

FIG. 3. Spatio-temporal grid used for the finite-difference time-domain calculations highlighting the discretization of the electric field, magnetic field, electric current density, and magnetic current density.

observed in the positive-index cases is a kink in the electric field at the dielectric-vacuum interface, which arises from the contra-directional phase velocities of the portions of the electromagnetic pulse in the slab and vacuum (due to the difference in the sign of $\mathrm{Re}[\underline{n}]$ in the dielectric and vacuum). Corresponding instantaneous force densities exerted by the pulse onto negative-index slabs without and with loss are depicted in Figs. 5(b) and 5(d), respectively. As shown in Fig. 6(a), the pulse transmitted through the lossless zero-index slab is also elongated and up-chirped. Unlike the positive-index and negative-index cases, however, the spatial oscillations of the pulse within the zero-index slab are not visible due to short extent of the pulse and the slab relative to the large effective wavelengths of the electromagnetic wave. The corresponding force density exerted by the pulse is shown in Fig. 6(b).

Using the electric field, magnetic field, electric current density, and magnetic current density calculated from the FDTD simulation, the force density, $\vec{f}(z,t)$, exerted by the pulse onto the slab is calculated using Eq. (26). The instantaneous pressure, $\vec{F}(t)$, is obtained by integrating the force density over the extent of the slab

$$\vec{F}(t) = \int_0^L \vec{f}(z,t)dz. \tag{40}$$

The corresponding momentum-per-unit-area imparted to the slab due to the Lorentz force

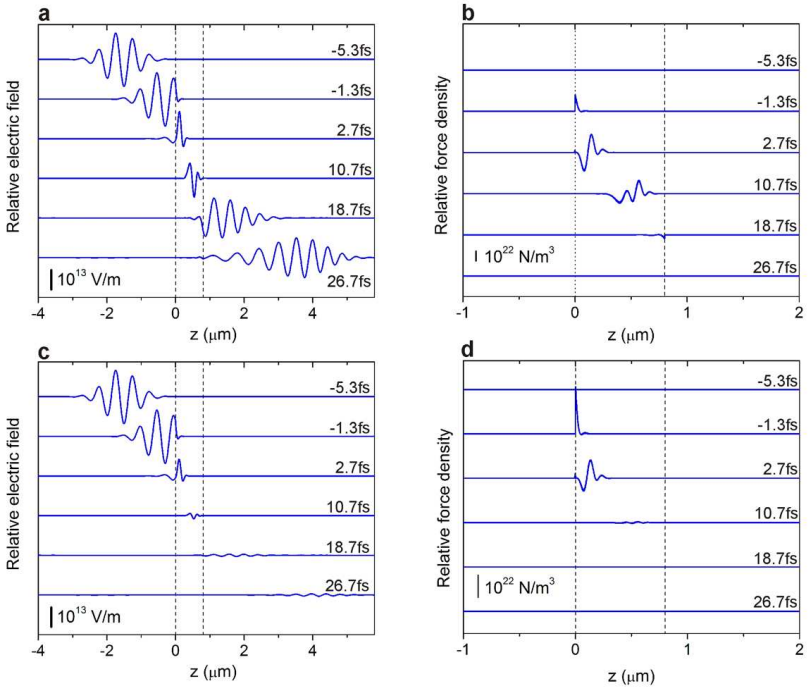

FIG. 4. Time sequence of the FDTD-calculated (a) electric field and (b) force density for a pulse incident onto a positive-index slab without loss (test case 1). FDTD-calculated (c) electric field and (d) force density for a pulse incident onto a positive-index slab with loss (test case 2). For clarity, the curves have been offset such that the horizontal asymptotic value of each curve corresponds to zero values. The pulse amplitude is normalized such that the total pulse power is 1 W. The slab has a length $L = 750\,\text{nm}$ and a mass $M = 1\,\text{kg}$. The dashed lines indicate the edges of the slab.

density, $\vec{p}_s(t)$, at a particular time t is given by

$$\vec{p}_s(t) = \int_{-\infty}^{t} \vec{F}(\tau) d\tau. \tag{41}$$

In addition to the momentum-per-unit-area imparted to the slab, we can calculate the momentum-per-unit-area carried by the pulse, $\vec{p}_p(t)$. The electric field and magnetic field calculated from the FDTD simulations are used to determine the electromagnetic momentum density of the pulse, $\vec{G}(z,t)$, via Eq. (24). The momentum-per-unit-area of the pulse, $\vec{p}_p(t)$, is then obtained by integrating the momentum density of the pulse for all z

$$\vec{p}_p(t) = \int_{-\infty}^{\infty} \vec{G}(z,t) dz. \tag{42}$$

Figures 7(a) and 7(b) show the instantaneous pressure and momentum-per-unit-area of

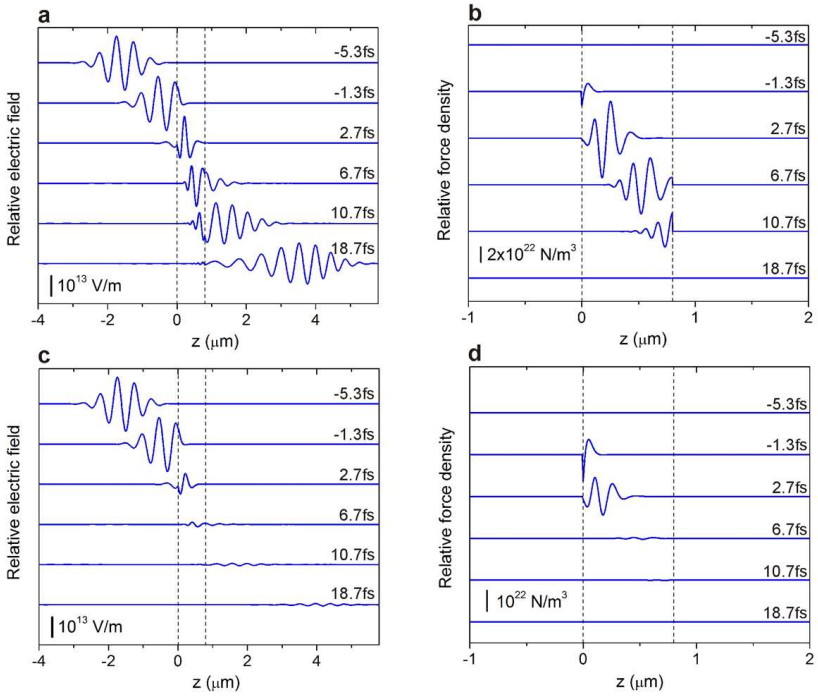

FIG. 5. Time sequence of the FDTD-calculated (a) electric field and (b) force density for a pulse incident onto a negative-index slab without loss (test case 1). FDTD-calculated (c) electric field and (d) force density for a pulse incident onto a negative-index slab with loss (test case 2). For clarity, the curves have been offset such that the horizontal asymptotic value of each curve corresponds to zero values. The pulse amplitude is normalized such that the total pulse power is 1 W. The dashed lines indicate the edges of the slab.

the pulse and the slab as the pulse traverses a dispersive positive-index, lossless slab. The pulse pushes on the slab when it enters, exerts successive positive and negative pressure alternating about zero when it is immersed in the slab, and pulls on the slab when it exits. The action of the pulse on the slab causes the slab momentum to increase from zero, plateau at a positive value, and then return to zero. As expected, use of the Abraham momentum density yields a decrease in the pulse momentum as the pulse moves from vacuum into the positive-index dielectric. The small fluctuations in the pulse momentum while the pulse is in the slab is due to dispersion of the slab. Changes in the pulse momentum are perfectly compensated by changes in the slab momentum, resulting in an always-constant total system momentum. When the pulse is incident onto the lossy positive-index slab, the pulse pushes

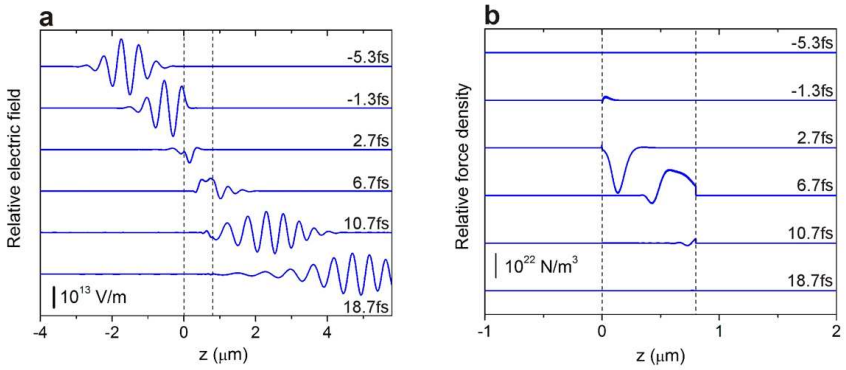

FIG. 6. Time sequence of the FDTD-calculated (a) electric field and (b) force density for a pulse incident onto a zero-index slab without loss (test case 5). For clarity, the curves have been offset such that the horizontal asymptotic value of each curve corresponds to zero electric field. The pulse amplitude is normalized such that the total pulse power is 1 W. The dotted lines indicate the edges of the slab.

on the slab upon entry and, due to absorption in the slab, exerts rapidly diminishing pressure after entry into the slab [Fig. 7(c)]. Absorption of the pulse in the slab means that the pulse cannot boost its momentum upon exit from the back of the slab. As a result, the slab gains and keeps all the initial momentum carried by the pulse [Fig. 7(d)]. As in the case of a lossless slab, the total system momentum is conserved at all times.

Changing the electromagnetic response of the slab from right-handed (positive-index) to left-handed (negative-index) does not significantly change how the pulse interacts with the slab. Like the case for the lossless positive-index slab, the pulse incident onto a lossless negative-index slab pushes upon entry and pulls upon exit [Fig. 8(a)], resulting in a slab momentum that initially increases from zero and then returns to zero [Fig. 8(b)]. The pulse momentum remains positive throughout its interaction with the slab. The positive electromagnetic momentum observed here also contradicts previous predictions of negative electromagnetic momentum in left-handed media [13]. The pulse momentum decreases from its initial value to a smaller, positive value and then returns back to its initial value upon exiting the slab. The total momentum of the system is always conserved. When loss is introduced to the negative index slab, the pulse simply pushes on the slab [Fig. 8(c)], transferring all its momentum to the slab in a way that still conserves the total momentum

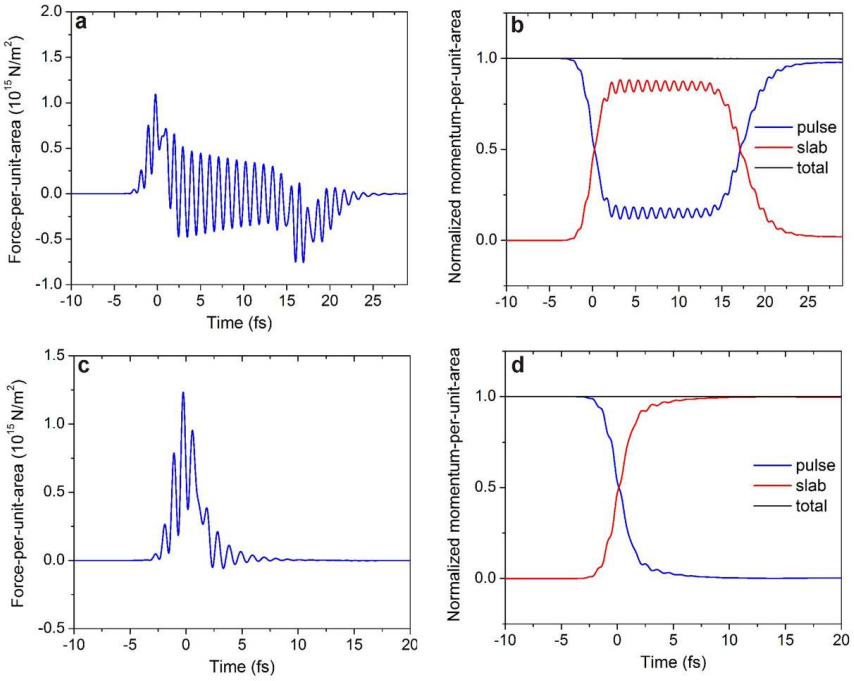

FIG. 7. (a) Instantaneous force-per-unit-area and (b) momentum-per-unit-area of the slab (red), pulse (blue), and system (black) for the case of a positive-index, lossless slab (test case 1). (c) Instantaneous force-per-unit-area and (d) momentum-per-unit-area of the slab (red), pulse (blue), and system (black) for the case of a positive-index, lossy slab (test case 2).

of the system [Fig. 8(d)].

A pulse traversing through a zero-index slab exerts oscillatory pressure throughout its interaction with the slab, with amplitudes exceeding those observed in the positive- and negative-index cases [Fig. 9(a)]. The large-amplitude pressure oscillations arise because the spatial periodicity of the carrier wave in the slab is elongated so that the fields are nearly constant over the extent of the pulse. The near-constant fields more efficiently exert force density on the slab, resulting in the large fluctuations in the pressure. When the pulse is fully immersed in the slab, the slab momentum hovers between approximately 60 % to 100 % and the pulse momentum between approximately 0 % to 40 % of the initial incident pulse momentum [Fig. 9(b)]. It should be noted that the magnitude of the pulse momentum in the slab is always less than the initial pulse momentum in vacuum.

We next consider the center-of-mass displacements of the pulse, the slab, and the entire

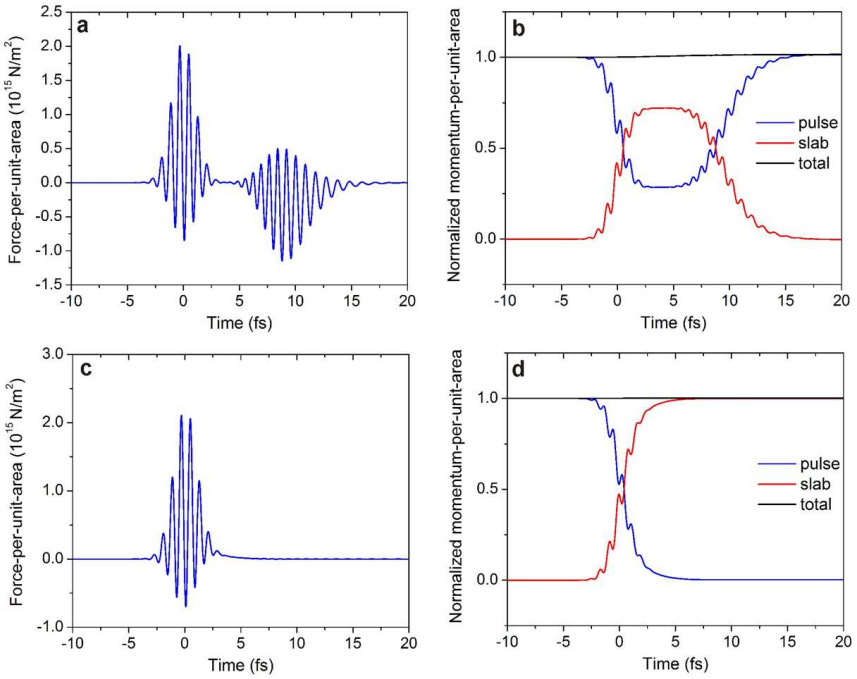

FIG. 8. (a) Instantaneous force-per-unit-area and (b) momentum-per-unit-area of the slab (red), pulse (blue), and system (black) for the case of a negative-index, lossless slab (test case 3). (c) Instantaneous force-per-unit-area and (d) momentum-per-unit-area of the slab (red), pulse (blue), and system (black) for the case of a negative-index, lossy slab (test case 4).

system when the pulse interacts with the slab. Using the FDTD-calculated field quantities, the mass density of the pulse, $\rho(z,t)$, is calculated from Eq. (38). For a pulse that is uniform over a cross-sectional area, $A = 1\,\mathrm{m}^2$, the mass of the pulse at any time is

$$m(t) = A \int_{-\infty}^{\infty} \rho(z,t) dz. \tag{43}$$

The center-of-mass of the pulse is then given by

$$z_p(t) = \frac{A \int_{-\infty}^{\infty} \rho(z,t) z dz}{m(t)}. \tag{44}$$

In general, a pulse incident onto a slab will cause regions of compression and rarefaction, which propagate across the slab at a speed less than c. We simplify our analysis by treating the limiting case where the slab is sufficiently rigid and massive such that elastic interactions between adjacent molecules may be ignored. We examine the center-of-mass of the slab, which can be displaced by both the momentum-per-unit-area $p_s(t)$ applied by the pulse and

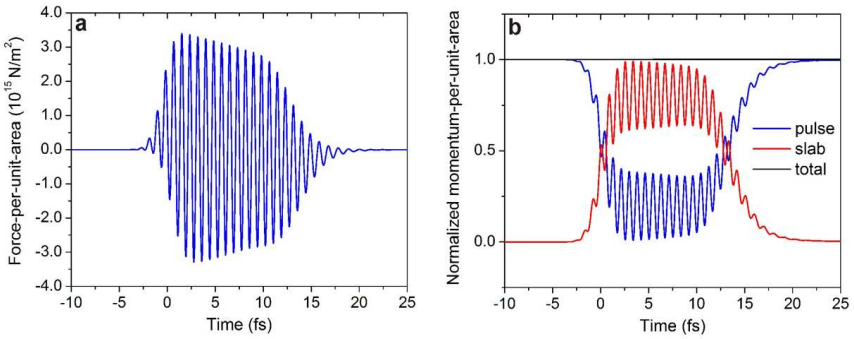

FIG. 9. (a) Instantaneous force-per-unit-area and (b) momentum-per-unit-area of the slab (red), pulse (blue), and system (black) for the case of a zero-index, lossless slab (test case 5).

the slab mass distribution shift due to absorption of the pulse in the slab. We define m_0 and M_0 to be the initial mass of the pulse and the slab, respectively, before the pulse has entered the slab. Conservation of mass is imposed in the simulations by maintaining a fixed total system mass

$$m_0 + M_0 = m(t) + M(t) \tag{45}$$

where $M(t)$ is the time-dependent mass of the slab. Absorption of the pulse in the slab is modeled by incrementally transferring mass from the pulse to the slab over the course of the simulation. At each time step of the simulation, the incremental decrease in the mass of the pulse $\Delta m(t+\Delta t) = m(t) - m(t+\Delta t)$ is distributed over the instantaneous normalized mass density profile of the pulse to yield an absorbed mass density over the time increment Δt

$$\rho_a(z, t+\Delta t) = \Delta m(t+\Delta t)\frac{\rho(z, t+\Delta t)}{m(t+\Delta t)}. \tag{46}$$

The absorbed mass density over the time increment Δt is added to the slab mass density at the previous time step, $\rho_s(z,t)$, to yield an updated slab mass density at $t+\Delta t$ given by

$$\rho_s(z, t+\Delta t) = \rho_s(z,t) + \rho_a(z, t+\Delta t) \tag{47}$$

where $M(t+\Delta t) = \int_{-\infty}^{\infty} \rho_s(z, t+\Delta t)dz$. At a given moment in time, the slab center-of-mass displacement is calculated from

$$z_s(t) = \frac{A\int_{-\infty}^{t} p_s(\tau)d\tau + A\int_{-\infty}^{\infty} \rho_s(z,t)(z - L/2)dz}{M(t)}, \tag{48}$$

where the first and second terms in the numerator of Eq. (48) describe the shift in the center-of-mass of the slab due to momentum transfer from the pulse to the slab and mass transfer from the pulse to the slab, respectively. Based on the pulse and slab center-of-mass displacements, we calculate the center-of-mass displacement of the total system using

$$z_{sys}(t) = \frac{m(t)z_p(t) + M(t)z_s(t)}{M(t) + m(t)}. \tag{49}$$

As shown in Fig. 10, a pulse incident on a slab causes a forward displacement of the slab, regardless of the refractive index of the slab. Similar center-of-mass trajectories are observed for the lossless positive-index, negative-index, and zero-index cases, where the slab center-of-mass displacements are initially zero, increase linearly while the pulse propagates through the slab, and settle at a constant positive value after the pulse exits. When the pulse is absorbed in either the positive-index or negative-index lossy slabs, the slab center-of-mass displacement ramps up from zero and, due to complete transfer of the incident pulse momentum to the slab, linearly increases indefinitely.

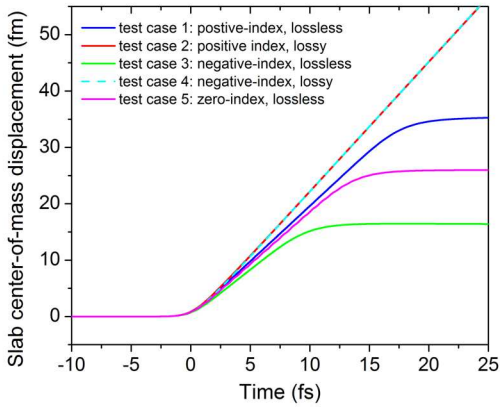

FIG. 10. Slab center-of-mass displacement for a pulse incident onto a slab for all five test cases studied.

Based on the slab and pulse center-of-mass displacements, we calculate the system center-of-mass displacement. As seen in Fig. 11, the system center-of-mass displacement for a pulse incident onto a slab, for all values of complex refractive index, increases linearly for all time, meaning that the system center-of-mass velocity is always conserved. The same holds true in the absence of impedance matching. In Appendix B, we perform similar analysis for a

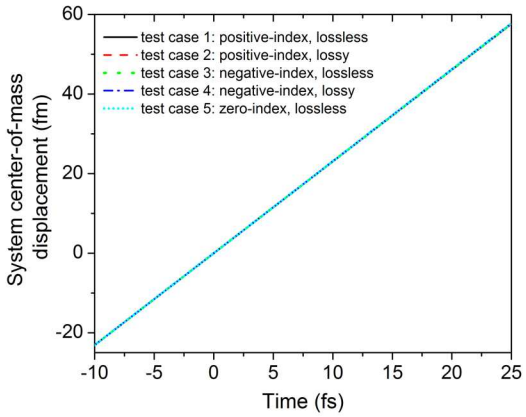

FIG. 11. System center-of-mass displacement for a pulse incident onto a slab for all five test cases studied.

test case consisting of a non-impedance-matched slab that is also dispersive, negative-index, and lossy, and show that momentum and system center-of-mass velocity are conserved. Thus, within the limits of the rigid and massive slab assumption, the postulates we have constructed to describe the behavior and interaction of electromagnetic fields in ponderable media are consistent with conservation of center-of-mass velocity.

CONCLUSION

In conclusion, we have proposed a set of postulates to describe the mechanical interaction between a plane-wave electromagnetic pulse and a dispersive, dissipative slab having a refractive index of arbitrary sign as a result of being left- or right-handed. The postulates include the Abraham electromagnetic momentum density, a generalized Lorentz force law, and a dynamic model for absorption-driven mass transfer from the pulse to the slab medium. These opto-mechanical mechanisms are incorporated into one-dimensional, finite-difference time-domain algorithm solving Maxwell's equations. The consistency of the postulates with conservation laws of momentum and mass was verified through a series of test cases where the complex refractive index of the slab spans a wide range of values. Consistency with conservation of momentum for all explored test cases validates the Abraham electromagnetic momentum density and the generalized Lorentz force law, while consistency with conser-

vation of center-of-mass velocity validates the proposed model for pulse mass density and dynamic mechanism for mass transfer from the pulse to the dissipative, dispersive medium.

APPENDIX A: APPLICATION OF THE MINKOWSKI MOMENTUM DENSITY AND ITS ASSOCIATED FORCE DENSITY TO DESCRIBE OPTO-MECHANICAL INTERACTIONS

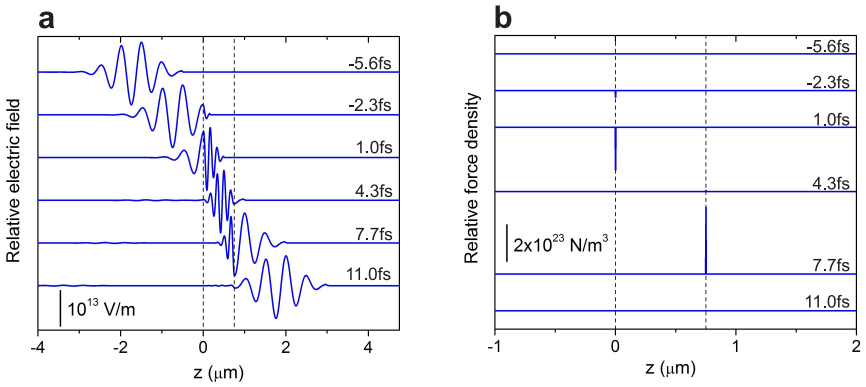

FIG. 12. Time sequence of the FDTD-calculated (a) electric field and (b) force density for a pulse incident onto an impedance-matched, non-dispersive, positive-index slab without loss. The force density is calculated using the form of the force density given by Eq. (54), which corresponds to the Minkowski momentum density. For clarity, the curves have been offset such that the horizontal asymptotic value of each curve corresponds to a zero quantity. The pulse amplitude is normalized such that the total pulse power is 1 W. The slab has a length $L = 750\,\text{nm}$ and a mass $M = 1\,\text{kg}$. The dotted lines indicate the edges of the slab.

We examine the implications of selecting the Minkowski momentum density and its associated force density, in addition to the postulates of Maxwell's equations [Eqs. (1) and (2)], the Poynting theorem [Eq. (33)], and the electromagnetic mass density [Eq. (37)], to describe an electromagnetic plane-wave pulse normally incident from free-space onto a flat slab. The Minkowski momentum density is given by [4]

$$\vec{G} = \vec{D} \times \vec{B}. \tag{50}$$

To derive the corresponding force density, we use the form of the stress tensor associated

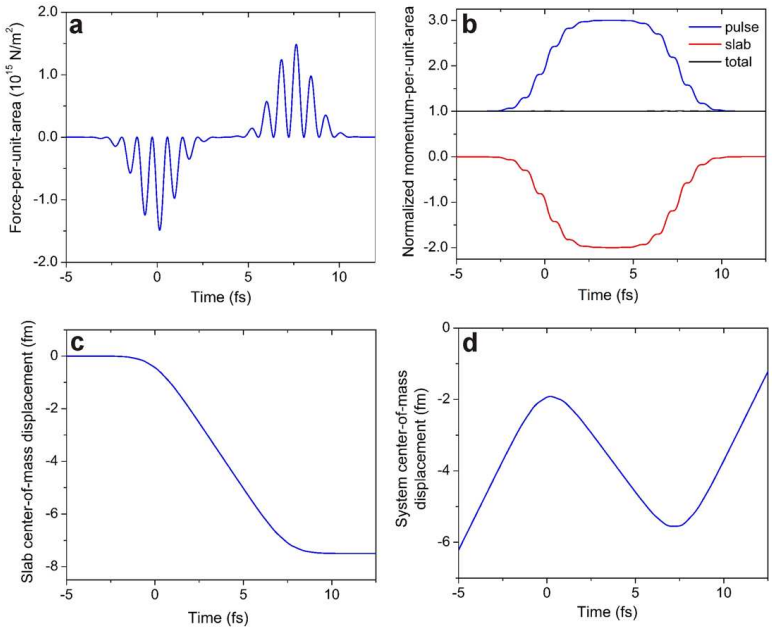

FIG. 13. (a) Instantaneous force density, (b) momentum-per-unit-area, (c) slab center-of-mass displacement, and (d) system center-of-mass displacement calculated for a pulse incident onto a lossless, non-dispersive, non-impedance-matched slab having a positive refractive index, using the Minkowski momentum density given by Eq. (50) and the force density given by Eq. (54).

with the Minkowski momentum density, given by [33, 34]

$$\bar{\bar{T}} = -\vec{D}\vec{E} - \vec{B}\vec{H} + \frac{1}{2}(\vec{E}\cdot\vec{D} + \vec{H}\cdot\vec{B})\bar{\bar{I}}. \tag{51}$$

Substitution of Eqs. (50) and (51) into the momentum continuity equation given by Eq. (27) yields

$$\vec{f} = -\frac{\partial}{\partial t}(\vec{D}\times\vec{B}) + \nabla(\vec{D}\vec{E} + \vec{B}\vec{H}) - \frac{1}{2}\nabla(\vec{E}\cdot\vec{D} + \vec{H}\cdot\vec{B}). \tag{52}$$

Invoking the Ampere-Maxwell law and Faraday's law, Eq. (52) can be re-written as

$$\begin{aligned}\vec{f} = \frac{1}{2}[&-\vec{E}\times(\nabla\times\vec{D}) + \vec{D}\times(\nabla\times\vec{E}) - (\vec{E}\cdot\nabla)\vec{D} + (\vec{D}\cdot\nabla)\vec{E} \\ &-\vec{H}\times(\nabla\times\vec{B}) + \vec{B}\times(\nabla\times\vec{H}) - (\vec{H}\cdot\nabla)\vec{B} + (\vec{B}\cdot\nabla)\vec{H}].\end{aligned} \tag{53}$$

When Eq. (53) is applied to the case of an electromagnetic plane-wave normally incident onto a flat slab, it simplifies to

$$\vec{f} = \frac{1}{2}[-\vec{E}\times(\nabla\times\vec{D}) + \vec{D}\times(\nabla\times\vec{E}) - \vec{H}\times(\nabla\times\vec{B}) + \vec{B}\times(\nabla\times\vec{H})]. \tag{54}$$

We apply the set of postulates to describe an electromagnetic pulse incident onto a lossless, impedance-matched, non-dispersive slab characterized by the parameters $\epsilon_\infty = 3$ and $\mu_\infty = 3$. Figures 12(a) and 12(b) show time sequences of the electric field and force density, respectively, as the pulse propagates through the slab. The force density exerted by the pulse is highly localized at the front and back surfaces of the slab, in contrast to the spatially-distributed force density distributions calculated using Eq. (26). As shown in Fig. 13(a), the pulse initially exerts a pull on the slab upon entry and then exerts a push of equivalent magnitude upon exit. As expected, application of the Minkowski form of the momentum density results in a pulse momentum-per-unit-area that increases as the pulse enters the slab from vacuum, as shown in Fig. 13(b). Changes in the pulse momentum-per-unit-area are compensated by equal and opposite changes in the slab momentum-per-unit-area, resulting in a global momentum that is conserved for all time. Due to the negative and then positive momentum exerted by the pulse, the slab center-of-mass displacement is initially zero, decreases linearly as the pulse enters and travels through the slab, and then remains at a fixed negative value after the pulse exits, as shown in Fig. 13(c). As shown in Fig. 13(d), the system center-of-mass displacement initially increases before the pulse enters the slab, then decreases while the pulse is in the slab, and finally increases again after the pulse leaves the slab. Notably, the system center-of-mass velocity is not conserved. The combination of the Minkowski momentum density [Eq. (50)] and its corresponding force density [Eq. (53)] has therefore been shown to satisfy global conservation of momentum, but, for the test case studied here, has been also shown to violate conservation of center-of-mass velocity.

APPENDIX B: ELECTROMAGNETIC PULSE INCIDENT ONTO A NON-IMPEDANCE-MATCHED, DISPERSIVE, DISSIPATIVE SLAB

Here, we apply our postulates to examine the case where an electromagnetic pulse is incident from free space onto a slab that is not impedance-matched. The parameters of the slab are selected to be $\epsilon_\infty = 1$, $\mu_\infty = 1$, $\omega_{pe} = 5.2 \times 10^{15}\,\mathrm{rad}/s$, $\omega_{pm} = 6.7 \times 10^{15}\,\mathrm{rad}/s$, $\Gamma_e = 5.0 \times 10^{14}\,\mathrm{rad}/s$, and $\Gamma_m = 1.0 \times 10^{14}\,\mathrm{rad}/s$. Over the bandwidth of the incident pulse, the selected parameters describe a material that is non-impedance-matched ($\underline{\epsilon}_r \neq \underline{\mu}_r$), dissipative ($\mathrm{Im}[\underline{\epsilon}_r],\ \mathrm{Im}[\underline{\mu}_r] > 0$), and has real part of the refractive index that is negative ($\mathrm{Re}[\underline{\epsilon}_r],\ \mathrm{Re}[\underline{\mu}_r] < 0$). Figure 14(a) shows a time sequence of the electric field as the pulse

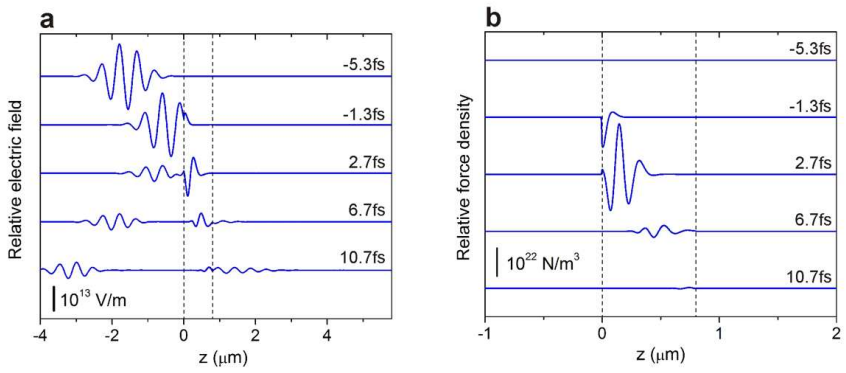

FIG. 14. Time sequence of the FDTD-calculated (a) electric field and (b) force density for a pulse incident onto a non-impedance-matched, negative-index slab with loss. For clarity, the curves have been offset such that the horizontal asymptotic value of each curve corresponds to zero values. The pulse amplitude is normalized such that the total pulse power is 1 W. The slab has a length $L = 750\,\text{nm}$ and a mass $M = 1\,\text{kg}$. The dotted lines indicate the edges of the slab.

is incident from free space onto the slab. Contrary to the other cases studied, a portion of the incident pulse reflects from the front face of the slab. A kink in the electric field at the interface between the free space and slab arises from the contra-directional phase velocities of the components of the pulse in free space and slab regions. The portion of the pulse that transmits through the front face of the slab is attenuated as it propagates through the slab, resulting in a weak transmitted pulse through the back of the slab. The force density exerted by the pulse is shown in Fig. 14(b). As shown in Fig. 15(a), the pulse pushes on the slab, with the greatest pressure exerted when the incident pulse initially interacts with the front face of the slab. The pulse momentum-per-unit-area is initially positive and then becomes negative after reflecting from the slab, as shown in Fig. 15(b). The negative momentum-per-unit-area arises because the incident pulse is split into reflected and transmitted components carrying momentum in the backward and forward directions, respectively. In this case, the negative momentum carried by the reflected pulse component exceeds the positive momentum carried by the transmitted component, resulting in a net negative momentum-per-unit-area. The slab momentum-per-unit-area increases from zero to a positive value exceeding the initial positive momentum-per-unit-area carried by the incident pulse. As a result, the total system momentum-per-unit-area is always conserved.

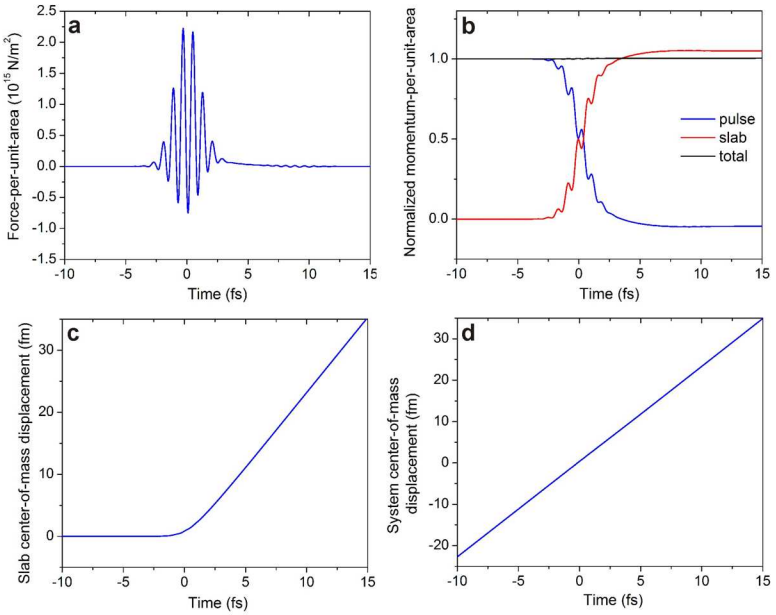

FIG. 15. (a) Instantaneous force density, (b) momentum-per-unit-area, (c) slab center-of-mass displacement, and (d) system center-of-mass displacement calculated for a pulse incident onto a dissipative, dispersive, non-impedance-matched slab having a negative real part of its refractive index.

As shown in Fig. 15(c), the slab center-of-mass displacement is initially zero and, due to the momentum imparted by the pulse onto the slab, linearly increases indefinitely. Despite reflection from the slab, Fig. 15(d) shows that the system center-of-mass displacement is always linear, meaning that the system center-of-mass velocity is always conserved. Thus, even in the absence of simplifying impedance-matching assumptions, Maxwell's equations, the Abraham momentum density, a generalized Lorentz force law, the Poynting theorem, and the mass transfer model provide a complete description of pulse interaction with a ponderable slab that is consistent with both conservation of global momentum and center-of-mass velocity.

ACKNOWLEDGMENTS

We acknowledge helpful discussions with M. Mansuripur and J. Weiner. KJC acknowledges support from the Natural Sciences and Engineering Council of Canada Discovery

Grant 366136.

[1] J. C. Maxwell, *A Treatise on Electricity and Magnetism, Volume 2* (Dover, 1891).

[2] P. N. Lebedev, "Untersuchungen über die druckkräfte des lichtes," Ann. Phys. **6**, 433–458 (1901).

[3] E. F. Nichols and G. F. Hull. "A preliminary communication on the pressure of heat and light radiation," Phys. Rev. **13**, 307–320 (1901).

[4] H. Minkowski, "Die Grundgleichungen für die elektromagnetischen Vorgänge in bewegten Körpern," Nachr. Ges. Wiss. Goettingen, Math.-Phys. Kl. 53–111 (1908).

[5] K. J. Chau and H. J. Lezec, "Re-visiting the Balazs thought experiment in the presence of loss: electromagnetic-pulse-induced displacement of a positive-index slab having arbitrary complex permittivity and permeability," Appl. Phys. A **105**, 267–281 (2011).

[6] M. Abraham, "Zur Elektrodynamik bewegter Körper," R. C. Circ. Mat. Palermo **28**, 1–28 (1909).

[7] R. N. C. Pfeifer, T. A. Nieminen, N. R. Heckenberg, and H. Rubinsztein-Dunlop, "Momentum of an electromagentic wave in dielectric media," Rev. Mod. Phys. **79**, 1197–1216 (2007).

[8] P. Penfield Jr. and H. A. Haus, *Electrodynamics of Moving Media* (M.I.T., 1960).

[9] S. R. dr Groot and L. G. Suttorp, *Foundations of Electrodynamics* (North Holland, 1972).

[10] R. Peierls, "The momentum of light in a refracting medium," Proc. R. Soc. Lond. A **347**, 475–491 (1976).

[11] P. W. Milonni and W. Boyd, "Recoil and photon momentum in a dielectric," Laser Phys. **15**, 1–7 (2005).

[12] S. Stallinga, "Energy and momentum of light in dielectric media," Phys. Rev. E **73**, 026606 (2006).

[13] B. A. Kemp, J. A. Kong, and T. M. Grzegorczyk, "Reversal of wave momentum in isotropic left-handed media," Phys. Rev. A **75**, 053810 (2007).

[14] P. L. Saldanha, "Division of the momentum of electromagnetic waves in linear media into electromagnetic and material parts," Opt. Express **18**, 2258–2268 (2010).

[15] J. P. Gordon, "Radiation forces and momenta in dielectric media," Phys. Rev. A **8**, 14–21 (1973).

[16] N. L. Balazs, "The energy-momentum tensor of the electromagnetic field inside matter," Phys. Rev. **91**, 408–411 (1953).

[17] A. Einstein, "The principle of conversation of motion of the center of gravity and the inertia of energy," Ann. Phys. **20**, 627–633 (1906).

[18] V. Veselago, "The electrodynamics of substances with simultaneously negative values of ϵ and μ," Sov. Phys. Usp. **10**, 509–514 (1968).

[19] R. A. Shelby, D. R. Smith, and S. Schultz, "Experimental verification of a negative index of refraction," Science **292**, 77–79 (1999).

[20] G. Dolling, M. Wegener, C. M. Soukoulis, and S. Linden, "Negative-index metamaterial at 780 nm wavelength," Opt. Lett. **32**, 53–55 (2007).

[21] V. M. Shalaev, W. Cai, U. K. Chettiar, H. -K. Yuan, A. K. Sarychev, V. P. Drachev, and A. V. Kildishev, "Negative index of refraction in optical metamaterials," Opt. Lett. **30**, 3356–3358 (2005).

[22] H. J. Lezec, J. A. Dionne, and H. A. Atwater, "Negative refraction at visible frequencies," Science **316**, 430–432 (2007).

[23] M. Mansuripur and A. R. Zakharian, "Energy, momentum, and force in classical electrodynamics: application to negative-index media," Proc. SPIE OP101, 73920Q-1 (2009).

[24] M. Mansuripur and A. R. Zakharian, "Energy, momentum, and force in classical electrodynamics: application to negative-index media," Opt. Commun. **283**, 4594–4600 (2010).

[25] R. W. Ziolkowski and E. Heyman, "Wave propagation in media having negative permittivity and permeability," Phys. Rev. E **64**, 056625 (2001).

[26] R. W. Ziolkowski, "Superluminal transmission of information through an electromagnetic metamaterial," Phys. Rev. E **63**, 046604 (2001).

[27] R. A. Depine and A. Lakhtakia, "A new condition to identify isotropic dielectric-magnetic materials displaying negative phase velocity," Microw. Opt. Technol. Lett. **41**, 315–316 (2004).

[28] A. Einstein and J. Laub, "On the ponderomotive forces exerted on bodies at rest in the electromagnetic field," Ann. Phys. **26**, 541–550 (1908).

[29] M. Mansuripur, "Radiation pressure and the linear momentum of the electromagnetic field in magnetic media," Opt. Express **15**, 13502–13518 (2007).

[30] M. Mansuripur and A. R. Zakharian, "Maxwell's macroscopic equations, the energy-momentum postulates, and the Lorentz law of force," Phys. Rev. E **79**, 026608 (2009).

[31] M. Mansuripur, "Resolution of the Abraham-Minkowski controversy," Opt. Commun. **283**, 1997–2005 (2010).

[32] W. Shockley and R. P. James, ""Try simplest cases" discovery of "hidden momentum" forces on "magnetic currents"," Phys. Rev. Lett. **18**, 876–879 (1967).

[33] I. Brevik, "Experiments in phenomenological electrodynamics and the electromagnetic energy-momentum tensor," Phys. Rep. **52**, 133–201 (1979).

[34] B. A. Kemp, "Resolution of the Abraham-Minkowski debate: implications for the electromagnetic wave theory of light in matter," J. Appl. Phys. **109**, 111101 (2011).

[35] R. Ruppin, "Electromagnetic energy density in a dispersive and absorptive material," Phys. Lett. A **299**, 309–312 (2002).

[36] R. Loudon, "The propagation of electromagnetic energy through an absorbing dielectric," J. Phys. A **3**, 233–245 (1970).